# Ultrasound Echolocation using Accurate Gaussian Process Distance Fields

Cedric Le Gentil*, Othmane-Latif Ouabi†‡, Lan Wu*, Cedric Pradalier‡ and Teresa Vidal-Calleja*
*Robotics Institute, University of Technology Sydney, Australia
Email: {cedric.legentil; lan.wu-2; teresa.vidalcalleja }@uts.edu.au
†Sysnav, France
Email: othmane.ouabi@sysnav.fr
‡International Research Lab 2958 Georgia Tech-CNRS, France
Email: cedricp@georgiatech-metz.fr

***Abstract*— This paper introduces a novel method to estimate distance fields from noisy point clouds using Gaussian Process (GP) regression. Distance fields, or distance functions, gained popularity for applications like point cloud registration, odometry, SLAM, path planning, shape reconstruction, etc. A distance field provides a continuous representation of the scene and is defined as the shortest distance from any query point and the closest surface. The key concept of the proposed method is a *reverting* function used to turn a GP-inferred occupancy field into an accurate distance field. The reverting function is specific to the chosen GP kernel. This work provides the derivation of the proposed GP distance field. The level of accuracy of the proposed approach allows for novel applications that rely on precise distance estimation. This work presents an echolocation method using ultrasonic-guided waves sensing metallic structures. This method leverages the proposed distance field in physics-based models to simulate the signal propagation and compare it with the actual signal received. Both simulated and real-world experiments are conducted to demonstrate the soundness of our method.**

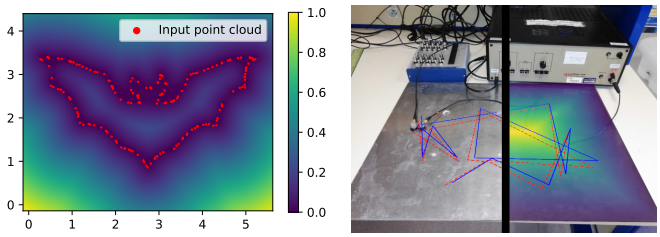


Fig. 1. Illustration of the proposed GP-based distance field. Given a point cloud, the proposed method successfully interpolates between the data points and provides an accurate distance field (left). The right image shows a real-world application for echolocation on metallic structures using an ultrasonic emitter-receiver (ground truth trajectory in blue, estimated trajectory in dashed red, and partial overlay of the GP-based distance field).

## I. Introduction

Robotics perception is a key component of any successful robotic system operating in the real world. The ability to sense and interpret the surrounding environment is crucial for navigation, planning, and overall systems performance. The choice of map representation to model the environment plays a vital role in the perception process. There exist many representations, each with its own specific set of applications. For example, dense 3D geometric point clouds are often used for lidar Simultaneous Localisation And Mapping (SLAM), while abstract sparse semantic maps are great tools for high-level decision-making. This paper introduces a novel continuous distance field representation based on Gaussian Process (GP) regression for an application in echolocation.

A distance field is a continuous function over a given space $\mathbb{R}^m$ that maps a query point $\mathbf{x}$ with the distance $d$ to the nearest object. In this paper, we will use the term *surface* to denote the outer layer of all the objects in the scene. For some regular-shaped objects, the surface can be represented with a *parametric* or *implicit* function that equals zero on the surface. The knowledge of such a function (eg., $ax + by + cz + w = 0$ for an infinite plane) may lead to a closed-form expression of the distance field. In the general case, the surface function and the distance field are not explicitly known and in the context of robotics perception, surfaces are often represented with discrete samples in the form of noisy point clouds. Inspired by Gaussian Process Implicit Surface (GPIS) [1] and LogGPIS [2, 3], the proposed method leverages kernel-based GP regression [4] as a framework for interpolation between the surface samples and generates an *occupancy field* over the space. This occupancy field is then transformed into a distance field by applying a *reverting* function deduced from the GP covariance kernel. As illustrated in Fig. 1, this approach produces an accurate continuous Euclidean distance field with interpolation capabilities alleviating drawbacks from other representations [2, 5].

Our method allows for new distance field applications beyond the typical point cloud-based observations for odometry, mapping and planning [3] thanks to its improved accuracy. We demonstrate the use of Ultrasonic Guided Waves (UGWs) with co-located, omnidirectional emitter-receivers on metallic plates for robotic navigation and inspection. The availability to query accurate distances with the nearest surface allows for the use of physics-based models of wave propagation in the measurement model of the proposed echolocation framework. Similarly to [6], we rely on the comparison between the actual echoes of the excitation signal and simulated received measurements.

In summary, the contributions of this work are the derivation of a novel GP-based distance field and its integration into a global localisation framework using UGWs.

## II. Gaussian Process distance fields

Considering a surface $\mathcal{S}$ in Euclidean space $\mathbb{R}^m$, let us define the distance field $d(\mathbf{x})$ with $\mathbf{x} \in \mathbb{R}^m$ as a scalar-valued continuous function that represents the shortest distance between the input $\mathbf{x}$ and the surface $\mathcal{S}$. Such a function is a solution to the Eikonal equation

$$|\nabla d(\mathbf{x})| = 1 \quad \text{with} \quad d(\mathbf{x}) = 0 \iff \mathbf{x} \in \mathcal{S}. \tag{1}$$

Given a set of points $\mathbf{X} = \{\mathbf{x}_1, \cdots, \mathbf{x}_N\}$ on the surface, the aim is to estimate the Euclidean distance $\hat{d}$. Unfortunately, as per its non-linear nature, the Eikonal equation (1) does not possess a known general closed-form solution. In this work, we approach the distance field estimation under the scope of *occupancy field* and GP regression [4] (c.f. Appendix I for a brief background on GP regression). Let us consider a set of points $\mathbf{x}_i$ on the surface $\mathcal{S}$ and a continuous scalar-valued field over $\mathbb{R}^m$ that we refer to as the occupancy field $o(\mathbf{x})$. Arbitrarily, we set the observed value of the occupancy field to one at the locations $\mathbf{x}_i \in \mathcal{S}$[1]. By modelling the occupancy field with a GP using a covariance kernel $k_o$, $o(\mathbf{x}) \sim \mathcal{GP}\left(0, k_o\left(\mathbf{x}, \mathbf{x}'\right)\right)$, we can infer the occupancy at any point $\mathbf{x} \in \mathbb{R}^m$:

$$\hat{o}(\mathbf{x}) = \mathbf{k}_o(\mathbf{x}, \mathbf{X}) \left(\mathbf{K}_o(\mathbf{X}, \mathbf{X}) + \sigma_o^2 \mathbf{I}\right)^{-1} \mathbf{1}, \tag{2}$$

with $\mathbf{k}_o(\mathbf{x}, \mathbf{X})$ the covariance vector between the query point and the surface observations, and $\mathbf{K}_o(\mathbf{X}, \mathbf{X})$ the covariance matrix of the observations. By considering a monotonic, stationary, isotropic kernel with an infinite domain (i.e., a non-zero, distance-based kernel: $k_o\left(\mathbf{x}, \mathbf{x}'\right) \rightarrow {k_o}'(\|\mathbf{x} - \mathbf{x}'\|)$, let us define a *reverting* function $r$ as

$$r\left(k_o\left(\mathbf{x}, \mathbf{x}'\right)\right) = r\left({k_o}'(\|\mathbf{x} - \mathbf{x}'\|)\right) \triangleq \|\mathbf{x} - \mathbf{x}'\|. \tag{3}$$

The proposed distance field consists in applying this reverting function to the GP-inferred occupancy field in (2) as $\hat{d}(\mathbf{x}) = r\left(\hat{o}\left(\mathbf{x}\right)\right)$.

Our approach is related to heat-based distance methods like [7] and [2], but the analysis of this relationship is out of the scope of this paper due to space limitations. However, it is important to note that the proposed representation enables a wide range of applications similar to LogGPIS [3]: scan-registration odometry, mapping, path planning, etc. While the applications in [3] are based on distance fields, they only require the minima of the field to be at the location of the surface, and the maxima to be the furthest away from the surface. In other words, they do not require the field to be an accurate Euclidean distance field. The accuracy of our method enables novel applications that require the actual Euclidean distance such as the problem of echolocation (c.f. Section III).

[1]Note that this approach differs from the definitions of GPIS where the field is positive inside the object, negative outside, and the surface corresponds to the zero crossing of the field.

| | **Covariance kernel** $(k_o(d))$ | **Reverting function** $(r(o))$ |
|---|---|---|
| Rational quadratic | $\sigma^2 \left(1 + \frac{d^2}{2\alpha l^2}\right)^{-\alpha}$ | $\sqrt{2\alpha l^2 \left(\left(\frac{o}{\sigma^2}\right)^{-\frac{1}{\alpha}} - 1\right)}$ |
| Square exp. | $\sigma^2 \exp\left(-\frac{d^2}{2l^2}\right)$ | $\sqrt{-2l^2 \log\left(\frac{o}{\sigma^2}\right)}$ |
| Matérn $\nu = 1$ | $\sigma^2 \frac{\sqrt{2}d}{l} B\left(-\frac{\sqrt{2}d}{l}\right)$ | $\underset{d}{\operatorname{argmin}} \left\|o - k_o\left(d\right)\right\|^2$ |
| Matérn $\nu = 3/2$ | $\sigma^2 \left(1 + \frac{\sqrt{3}d}{l}\right) \exp\left(-\frac{\sqrt{3}d}{l}\right)$ | $\underset{d}{\operatorname{argmin}} \left\|o - k_o\left(d\right)\right\|^2$ |

TABLE I

Covariance kernels and associated reverting functions ($B$ is the modified Bessel function of the second kind).

### A. Intuitive interpretation

To provide the reader with an intuition about the proposed method, let us first consider a 1D scenario with only one noiseless data point on the surface. The inference of the occupancy field provided by (2) is then reduced to $\hat{o}(x) = k_o\left(x, x_1\right)$. In that scenario, the reverting kernel function provides the exact distance between the surface and the query point $x$. As illustrated in Fig. 2 (left and middle), if we consider a set of noisy points close to the surface instead of a single noiseless measurement, the shape of the occupancy field is similar to the ideal 1D noise-free case. Without loss of generality, our method extends this reasoning to higher dimensions assuming that the occupancy field along the normal vectors to the surface is equivalent to the 1D scenario (c.f. Fig. 2 right).

### B. Kernels and reverting functions

As aforementioned, the proposed method relies on the pair kernel/reverting function to accurately estimate the distance field. This subsection discusses the case of the Rational Quadratic (RQ) kernel, the Square Exponential (SE) kernel, and a few other kernels from the Matérn family. These kernels, in their isometric form, depend on the Euclidean distance between the two input vectors. Accordingly, via a simple change of variables, they can be expressed as a function of a non-negative scalar value $d = \|\mathbf{x} - \mathbf{x}'\|$. Table I shows different kernels as well as their reverting function (with $\sigma^2$ as the scaling factor, and $l$ the kernel's lengthscale). In the case of the RQ and SE, it is straightforward to find the reverting function with simple algebraic manipulations. Unfortunately, Matérn kernels do not all possess a known, closed-form reverting function. In these scenarios, the reverting "function" can be formulated as a single-value non-linear optimisation problem.

## III. Ultrasound Echolocation

We apply the proposed distance field to the problem of global localisation of a system consisting of an omnidirectional (no bearing information) ultrasonic emitter-receiver in contact with a metallic structure. Industrial applications include the automated long-range inspection of large metal structures [6]. The proposed distance field is used in the UGW measurement model of a Monte-Carlo localisation algorithm.

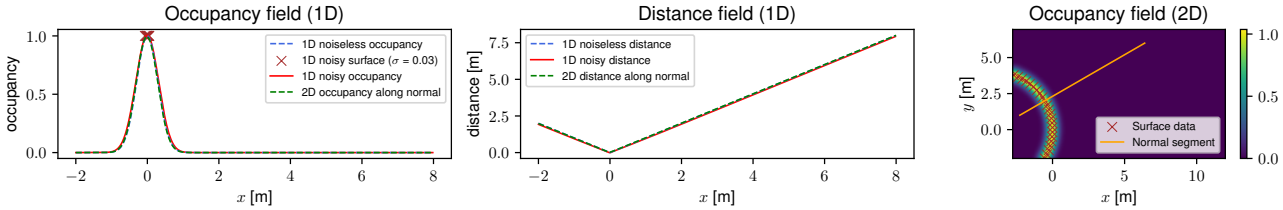


Fig. 2. Occupancy fields (1D and 2D) and corresponding distance according to the *reverting* function. The "2D" plots in the left and middle correspond, respectively, to the occupancy and distance along the normal segment (in orange) on the right. This figure is obtained using the square exponential kernel.

### A. Ultrasonic Guided Waves measurement model

Given an emitter-receiver, at every measurement step $i$, a time signal $s(t)$ is pulsed by the emitter to create an UGW that propagates radially around the emitter, *inside* the structure's material. Simultaneously, the receiver collects the measurement $z_i(t)$ that contains the ultrasonic echoes due to reflections of the excited wave on structural features (the boundaries $\mathcal{S}$ of a metal panel in our case study). These measurements can be modelled by relying on the *image source* model, which states that the reception of any echo can be interpreted as a signal originating directly from a fictive image source. The image sources' positions depend on the position of the actual emitter and the properties of the surface $\mathcal{S}$. With the assumption that the material is isotropic (i.e., wave propagation is the same in any direction), the propagation transfer is only a function of time and of the distance between the receiver and the image source. This results in the following measurement model:

$$\tilde{z}_i(t) = \sum_{\mathbf{p}\in\mathcal{I}(\mathbf{x}_i,\mathcal{S})} g(||\mathbf{p}-\mathbf{x}_i||,t) * s(t) + n_i(t), \quad (4)$$

where $s(t)$ is the excitation used to generate the UGW, $\mathbf{x}_i$ is the emitter position, $\mathcal{I}(\mathbf{x}_i,\mathcal{S})$ is the set of the image sources positions for a surface $\mathcal{S}$ and a real source position $\mathbf{x}$, $g(||\mathbf{p}-\mathbf{x}_i||,t)$ is the acoustic transfer function of the propagation medium[2], $n(t)$ is an additive Gaussian noise term that we assume temporally and spatially white, and $*$ denotes the convolution operation.

We generate a correlation signal between the measurement and the model to assess the likelihood that a *single* acoustic reflection occurred at any distance $d$ from the emitter-receiver with:

$$z'_i(d) = \frac{\langle z_i(t), \hat{z}(d,t)\rangle}{\sqrt{\langle z_i(t), z_i(t)\rangle\langle \hat{z}(d,t), \hat{z}(d,t)\rangle}}, \quad (5)$$

where $\hat{z}(d,t) = \hat{g}(2d,t) * s(t)$ is the expected signal containing an echo due to a reflection at a distance $d$, and $\langle .,. \rangle$ denotes the usual scalar product for time-continuous signals. We subsequently retrieve the envelope of the correlation signals with $e_i(d) = |z'_i(d) + j\mathcal{H}(z'_i)(d)|$, with $\mathcal{H}$ denoting the Hilbert transform operator. The envelope signal ranges between 0 and 1, and it presents a local maxima in $d$ if there is indeed a reflector at such distance, as illustrated in Fig. 3. The figure shows a distinguishable first echo that indicates the presence of a plate boundary at $0.08\,\mathrm{m}$ and late echoes that will be considered noise.

[2]A standard propagation model for an UGW propagating in a metal panel is $\hat{g}(r,\omega) \approx e^{-jk(\omega)r}/\sqrt{k(\omega)r}$, where $k(\omega)$ is the wavenumber of the major acoustic mode that usually has a non-linear dependency with respect to the pulsation $\omega$. More details on how to determine this relation given prior information on the plate material can be found in [8].

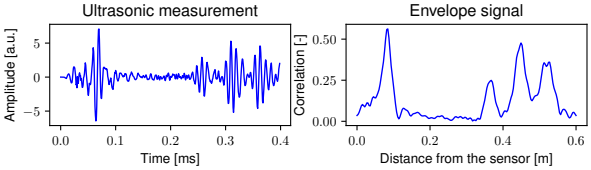


Fig. 3. Example of an acoustic measurement acquired on an aluminium plate (top plot) and the corresponding envelope signal obtained by correlating the measurement with a wave propagation model (bottom).

### B. Monte-Carlo echolocation

The objective here is to estimate the system's position $\mathbf{x}_i$ by relying on ultrasonic measurements, noisy odometry information, and given the map (the plate boundaries $\mathcal{S}$) in the form of a point cloud. To recover the position of a moving emitter-receiver, we rely on a particle filter, as in [6]. Such filters can usually provide satisfactory solutions to the localisation problem when the dynamic and observation models are non-linear, and the process and measurement noises are non-Gaussian [9], as in our case study. Yet, the method described in [6] can only be applied to metal panels with a rectangular shape. Hence, we propose a modification to the calculation of the particles' weights to make the approach applicable to arbitrary surface geometries, using the proposed GP-based distance field.

The modified localisation approach relies on the aforementioned envelope signals $e_i(d)$ to determine the likelihood of each of the particles in the filter. We propose the particle filter using the following expression for the particles' weight:

$$w_i^n = \eta \exp\left\{\alpha e_i(\hat{d}(\mathbf{x}_i^n)) - \beta \hat{d}^2(\mathbf{x}_i^n)\right\}, \quad (6)$$

where $\hat{d}(\mathbf{x}_i^n)$ is the GP-based distance of the $n$-th particle to the closest point on the surface $\mathcal{S}$ computed with (2) and the reverting function (3), $\eta$ is the normalization factor, and $\alpha$ and $\beta$ are positive parameters. The term in $\hat{d}^2(\mathbf{x}_i^n)$ is a prior used to account for the fact that the reception of the first ultrasonic echo is less likely at a larger distance. Note that a simpler measurement model that does not consider regularization can also be used, but it will be less robust to the presence of late echoes. The filter's output corresponds to the mean coordinates of the 50% best particles.

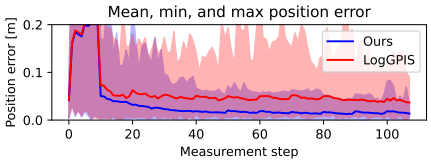


Fig. 4. Localisation results with the particle filter in the simulated scenario over 100 trials (solid line: average, coloured area: upper and lower bounds)

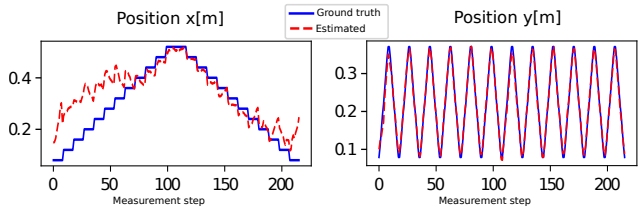


Fig. 5. Localisation results achieved with the particle filter in the real-world scenario.

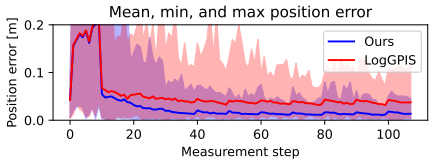


Fig. 6. Localisation results with the particle filter with real-world data over 100 trials (solid line: average, coloured area: upper and lower bounds)

## IV. Experiments

To validate our novel method, we test the particle filter with both LogGPIS and the proposed distance field (based on the RQ kernel, $\alpha = 100$) in simulation and in a real-world setting by using experimental ultrasonic measurements acquired on a metal panel. We consider the same setup for the two scenarios, where the UGW propagates in an aluminium metal panel with dimensions 600x450x6mm.

### A. Simulation

We create robot paths by randomly generating linear and rotational displacements between two successive measurement points. The excitation $s(t)$ is a two-tone burst sinusoidal wave at 100 kHz. The ultrasonic measurements are simulated using the image source model and an approximate wave propagation model, as presented in Section III-A. We also add Gaussian noise to the simulated data to maintain a fixed signal-to-noise ratio: SNR = 10dB. The noisy odometry inputs are generated by adding zero-mean Gaussian noise to the ground truth translation ($\sigma_{\mathrm{t}} = 0.3$cm) and rotational ($\sigma_{\mathrm{r}} = 0.05$rad) displacements, which are next presented as inputs to the particle filter.

Fig. 4 shows the average localisation results (over 100 trials). It can be observed that, despite imperfect initialization of the filter, the position estimate converges to the ground truth position with centimetre accuracy. Additionally, the proposed distance field significantly outperforms LogGPIS [3] which consistently presents an error level three times higher.

### B. Real-world

We acquire experimental measurements in a laboratory environment with the following procedure: an emitter/receiver pair of nearly collocated transducers, as depicted by Fig. 1 (right), is placed by hand on the vertices of a $9\times12$ regular grid whose positions are carefully recorded. For every position, the same excitation signal as in the previous scenario is used to generate the UGW, while the receiver collects the ultrasonic response. In total, 108 measurements were acquired. We simulate a "lawn-mower" trajectory as a robot path by using the theoretic displacement between the corresponding measurement positions as ground-truth odometry. In the same way, as in the previous scenario, we add zero-mean Gaussian noise to the resulting translation and rotational data to generate the noisy odometry inputs.

Fig. 5 shows the localisation results achieved in this scenario. It can be observed that the coordinate $y$ is estimated within centimetre accuracy, all along the trajectory. However, this is not the case for $x$, even though the estimate vaguely converges to the true $x$ before slightly diverging again. This can be explained by the fact that we only rely on the echo from the closest surface point for localisation (no bearing information), whereas most of the data has been acquired for sensor positions closer to a vertical boundary than a horizontal one. It is clear that the multiple echoes contained in the measurements should be leveraged in the future to improve the localisation accuracy in such scenarios. In Fig. 6, we sampled 100 trajectories by randomly selecting sequences of measurements from the original "lawn-mower" pattern to prevent the phenomenon mentioned above. Similarly to the simulated scenario, the proposed distance field provides a significantly better level of accuracy compared with LogGPIS [3]. Overall, these results support the relevance of using distance fields for localisation, without relying on geometric assumptions on the surface $\mathcal{S}$.

## V. Conclusion

In this paper, we presented a novel GP-based distance field estimation method. Using a point cloud as input, the proposed method first infers an occupancy value based on standard GP regression before applying a kernel reverting function. We demonstrated the potential of the proposed distance field via a framework for echolocation using UGWs.

In future work, we will tackle the UGW mapping problem. We will investigate the use of ultrasound measurements directly in the GP model to account for the information contained in multiple echoes of the excitation signal. This will result in more robustness with respect to noisy measurements.

## VI. Acknowledgment

Cedric Le Gentil and Teresa Vidal-Calleja are supported by the Australian Research Council Discovery Project under Grant DP210101336.

This work has been partially funded by the BugWright2 project, supported by the European Commission under grant agreement 871260 - BugWright2.

## REFERENCES

[1] O. Williams and A. Fitzgibbon, "Gaussian process implicit surfaces," 2007.

[2] L. Wu, K. M. B. Lee, L. Liu, and T. Vidal-Calleja, "Faithful euclidean distance field from log-Gaussian process implicit surfaces," *IEEE Robotics and Automation Letters*, vol. 6, no. 2, pp. 2461–2468, 2021.

[3] L. Wu, K. M. B. Lee, and T. Vidal-Calleja, "Log-GPIS-MOP: A unified representation for mapping, odometry and planning," *arXiv preprint arXiv:2206.09506*, 2022.

[4] C. E. Rasmussen and C. K. I. Williams, *Gaussian Processes for Machine Learning*. The MIT Press, 2006.

[5] J.-P. A. Ivan, T. Stoyanov, and J. A. Stork, "Online distance field priors for Gaussian process implicit surfaces," *IEEE Robotics and Automation Letters*, vol. 7, no. 4, pp. 8996–9003, 2022.

[6] O.-L. Ouabi, P. Pomarede, M. Geist, N. F. Declercq, and C. Pradalier, "Monte-carlo localization on metal plates based on ultrasonic guided waves," in *International Symposium on Experimental Robotics*. Springer, 2021, pp. 345–353.

[7] K. Crane, C. Weischedel, and M. Wardetzky, "Geodesics in heat: A new approach to computing distance based on heat flow," *ACM Transactions on Graphics (TOG)*, vol. 32, no. 5, October 2013.

[8] Z. Su and L. Ye, *Identification of Damage Using Lamb Waves: From Fundamentals to Applications*, 01 2009, vol. 48.

[9] S. Thrun, W. Burgard, D. Fox *et al.*, *Probabilistic robotics, vol. 1*. MIT press Cambridge, 2005.


## APPENDIX I
## GAUSSIAN PROCESS PRELIMINARIES

Let us consider an unknown signal $h(\mathbf{x}) \in \mathbb{R}$ with $\mathbf{x} \in \mathbb{R}^m$, and $Q$ noisy observations $y_i$ defined as

$$y_i = h\left(\mathbf{x}_i\right) + \eta_i, \quad \text{where } \eta_i \sim \mathcal{N}\left(0, \sigma^2\right). \tag{7}$$

where $i = (1, \cdots, Q)$. The goal is to infer the distribution (mean and variance) of $h$ for any given input $\mathbf{x}$.

By modelling the signal $h$ as a GP $h \sim \mathcal{GP}\left(0, k_h\left(\mathbf{x}, \mathbf{x}'\right)\right)$, with $k_h$ the covariance kernel function $k_h\left(\mathbf{x}, \mathbf{x}'\right) = \operatorname{cov}\left(h(\mathbf{x}), h(\mathbf{x}')\right)$, one can express occurrences of $h$ as a multivariate Gaussian distribution

$$\begin{bmatrix} \mathbf{y} \\ h(\mathbf{x}^*) \end{bmatrix} = \mathcal{N}\left(0, \begin{bmatrix} \mathbf{K}_h(\mathbf{X}, \mathbf{X}) + \sigma_h^2 \mathbf{I} & \mathbf{k}_h(\mathbf{x}^*, \mathbf{X})^\top \\ \mathbf{k}_h(\mathbf{x}^*, \mathbf{X}) & k_h\left(\mathbf{x}^*, \mathbf{x}^*\right) \end{bmatrix}\right), \tag{8}$$

where $\mathbf{y} = [y_1, \cdots, y_Q]^\top$, $\mathbf{x}^*$ is a query point, $\mathbf{k}_h(\mathbf{x}^*, \mathbf{X}) = [k_h\left(\mathbf{x}^*, \mathbf{x}_1\right), \cdots, k_h\left(\mathbf{x}^*, \mathbf{x}_Q\right)]$, and $\mathbf{K}_h(\mathbf{X}, \mathbf{X}) = [\mathbf{k}_h(\mathbf{x}_1, \mathbf{X})^\top, \cdots, \mathbf{k}_h(\mathbf{x}_1, \mathbf{X})^\top]$. By conditioning (8) with respect to the noisy observations, the mean and variance of $h(\mathbf{x}^*)$ are respectively computed as

$$\begin{aligned} \hat{h}(\mathbf{x}^*) &= \mathbf{k}_h(\mathbf{x}^*, \mathbf{X})\left(\mathbf{K}_h(\mathbf{X}, \mathbf{X}) + \sigma_h^2 \mathbf{I}\right)^{-1} \mathbf{y}, \quad \text{and} \\ \operatorname{var}(h(\mathbf{x}^*)) &= k_h\left(\mathbf{x}^*, \mathbf{x}^*\right) - \\ &\quad \mathbf{k}_h(\mathbf{x}^*, \mathbf{X})\left(\mathbf{K}_h(\mathbf{X}, \mathbf{X}) + \sigma_h^2 \mathbf{I}\right)^{-1} \mathbf{k}_h(\mathbf{x}^*, \mathbf{X})^\top. \end{aligned} \tag{9}$$